VIMPAC: Video Pre-Training via Masked Token Prediction and Contrastive Learning

Hao Tan*[1] Jie Lei*[1] Thomas Wolf[2] Mohit Bansal[1]
[1]UNC Chapel Hill [2]Huggingface
{haotan, jielei, mbansal}@cs.unc.edu; thomas@huggingface.co

Abstract

Video understanding relies on perceiving the overall global content and modeling its internal connections (e.g., causality, movement, and spatio-temporal correspondence). To learn these interactions, we apply a mask-then-predict pre-training task on the discretized video tokens generated via VQ-VAE. Unlike language, where the text tokens are more independent, neighboring video tokens typically have strong correlations (e.g., consecutive video frames usually look similar), and hence uniformly masking individual tokens will make the task too trivial to learn useful representations. To deal with this issue, we propose a block masking strategy where we mask neighboring video tokens in both spatial and temporal domains. We also add a contrastive learning objective to further capture the global content by predicting whether the video clips are sampled from the same video. We pre-train our model on uncurated videos and show that our pre-trained model can reach state-of-the-art results on several video understanding datasets (e.g., SSV2, Diving48). Lastly, we provide detailed analyses of the model scalability and pre-training method design.

1. Introduction

In recent years, state-of-the-art self-supervised methods have been exploring different directions for pre-training images and text representations, with Contrastive Learning (CL) providing strong results for vision representation learning [12, 13, 30, 47, 61], and Language Modeling (LM) becoming the de-facto standard in language pre-training [17, 40, 43, 70]. Interestingly, video understanding naturally combines both types of requirements. 2D processing along the spatial dimensions of the video bears similarity to image processing, while 1D processing along the temporal dimension often involves modeling sequential events and short range coherence.

Hence, in this work, we propose to combine both text and image representation learning approaches for improved video pre-training, taking advantage of recent advances in self-supervised methods of both fields. We name our method as VIMPAC: VIdeo pre-training via Masked token Prediction And Contrastive learning. From language research, we adopt a 'masked language model' pre-training objective [17] where a model is trained to reconstruct local masked regions in videos. From the computer vision world, we borrow a contrastive learning objective, specifically the InfoNCE [47] objective is applied on positive/negative video samples. While the masked language model objective encourages models to learn low-level semantics and sequential interaction, the contrastive loss provide a supervision for the model to learn more global and separable representations that are useful for many downstream tasks (e.g., action classification [10, 57]). However, unlike language which is composed of discrete tokens from a compact vocabulary, videos are typically represented as RGB pixels in an almost continuous, high dimensional vector space. Naively masking pixels in videos induces a prohibitive computation cost while also tending to over-emphasize local details. To overcome these issues, we introduce a block-masking scheme that simultaneously masking video tokens in a 3D spatio-temporal block.

We evaluate the performances of our method VIMPAC on several video understanding datasets, including two temporally-heavy tasks, SSV2 and Diving48 on which it achieves state-of-the-art results with regard to both self-supervised and supervised pre-training works, and a set of more spatially-heavy datasets, UCF101, HMDB51, and Kinetics-400, on which it also achieves competitive results. Overall, our contribution is 3-folds: (i) We apply the mask-then-predict task to video understanding and introduce the use of block masking. (ii) We propose a contrastive learning method which is able to achieve strong performance without spatial data augmentation. (iii) We empirically show that this method achieves strong performance on several video classification datasets, especially on temporally-heavy datasets, SSV2 and Diving48, where it sets new state-of-the-art results. We also present comprehensive ablation

*Equal contribution.

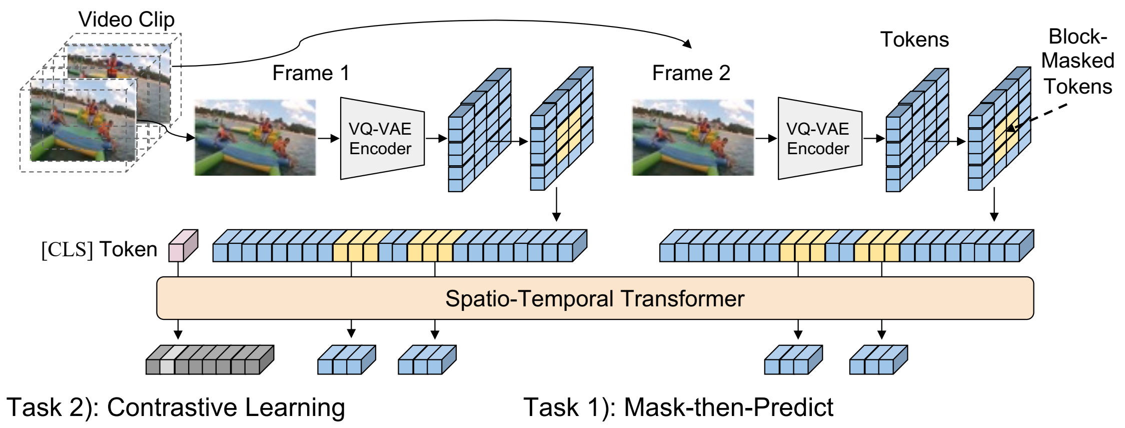

Figure 1. Overview of VIMPAC. Sampled video frames are discretized by VQ-VAE encoder into discrete tokens, which are then block-masked (in light yellow blocks). The model is self-supervised by two tasks: 1) *mask-then-predict* task predicts the masked tokens from their visible context; 2) *contrastive learning* task differentiates between positive and negative clips (details in Fig. 2) with [CLS] token feature. For brevity, we only show 2 frames with small token maps.

studies to analyze the aspects of our proposed approach.

2. Related Work

Generative and denoising methods seek to generate or reconstruct corrupted text/image/video tokens according to their empirical distributions. In generative and auto-regressive methods, next tokens are predicted given a causal context [11, 63] while denoising methods seek to reconstruct corrupted or masked tokens given an extended context [17, 51, 54]. In the case of images, generative approaches often operate on pixel space [6, 11, 36, 63, 71], which can be extremely expensive for larger input size like videos. Recently, discretizing images and videos with discrete variational auto-encoders (VQ-VAE), has been explored in generative setups [52, 53, 58, 64, 66, 69]. Based on this, we propose a block masking strategy to reduce the strong local correlation in neighboring video tokens. This 3D block masking strategy is inspired from recent span-masking schemes [34, 51] for language modeling. The concurrent work [4] explores using the VQ-VAE tokens as labels for masked patches in the image domain.

The other direction of research, which our framework combines, is discriminative methods. Traditionally, the objective is constructed around hand-crafted heuristics tasks like spatial arrangement, color, playback speed or frame order predictions [5, 18, 20, 24, 27, 41, 59, 68, 73]. A recent line of discriminative approaches is *contrastive learning* which aims at training a model to be able to recognize different views of the same image or video, as a way to learn general representations [8, 12, 13, 23, 29, 30]. This direction of research is reminiscent of sentence-order prediction tasks introduced in NLP [17, 40].

3. Methods

In this section, we present our proposed video pre-training method VIMPAC (Fig. 1) as well its detailed components. We first introduce the mask-then-predict task in Sec. 3.1, and then the contrastive learning task in Sec. 3.2. Lastly, we discuss how these two tasks are combined in Sec. 3.3. The model details are provided in the Appendix.

3.1. Mask-then-Predict Task

Suppose that a video clip input comprises T frames $\{f_1, f_2, \ldots, f_{\mathrm{T}}\}$, the mask-then-predict task learns video representations by predicting the masked contents from their spatio-temporal context. Denote the set of mask-token locations as M, we learn to predict the original tokens $\{x_{t,i,j}\}$ (see details below) by optimizing the negative log-likelihood:

$$\mathcal{L}_{\text{mask}} = -\frac{1}{|M|} \sum_{t,i,j \in M} \log p_{t,i,j} \left(x_{t,i,j} | \{x_{t',i',j'}\}_{t',i',j' \in M^{\mathrm{C}}} \right) \tag{1}$$

where M^{C} is the complement of M and thus indicates the unmasked context.

Block Masking For sampling tokens to mask, the original BERT methods proposes the i.i.d. (independent and identically distributed) random mask M_{iid} that constitutes of masked tokens:

$$M_{\text{iid}} = \{(t,i,j) \mid \mathcal{U}_{t,i,j}[0,1] < \xi\}, \tag{2}$$

where $\mathcal{U}_{t,i,j}[0,1]$ is the uniform distribution from 0 to 1. Intuitively, ξ is the expectation of masked-token ratio and

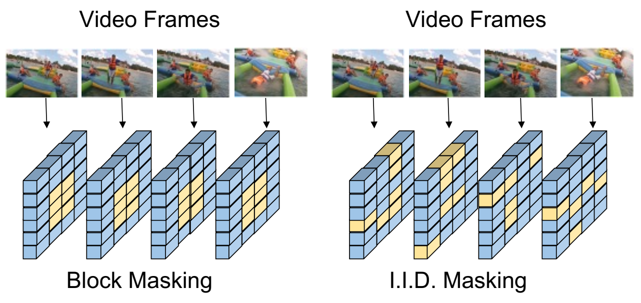

(a) Illustration of Block and I.I.D. Masking.

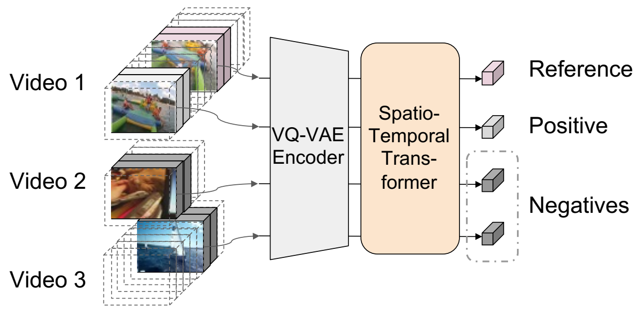

(b) Illustration of Contrastive Learning.

Figure 2. Illustration of pre-training tasks. *(a)*: block masking constructs the 3D-contiguous masking cube while i.i.d masking independently samples masked tokens. *(b)*: given the reference clip, the positive clip is uniformly sampled from the same video (video 1) while negative clips are sampled from other videos (video 2, 3). No spatial augmentations are applied to the raw video clips.

hence controls the difficulty of our mask-then-predict task. As shown in Sec. H.2, it is easy to infer a masked token from its direct spatio-temporal neighbours. To overcome this issue, we propose to use block masking (see Fig. 2 (a)), which masks continuous tokens inside spatio-temporal blocks. For each mask block B, we randomly sample lower ($B_{*,0}$) and upper boundaries ($B_{*,1}$) for each of the temporal (T), height (H), and width (W) dimensions. The final mask M_{block} is the union of them:

$$M_{\text{block}} = \bigcup_B [B_{T,0}, B_{T,1}] \times [B_{H,0}, B_{H,1}] \times [B_{W,0}, B_{W,1}]. \tag{3}$$

3.2. Contrastive Learning

Contrastive learning aims to distinguishing positive pairs from negative pairs (see Fig. 2 (b)). For each video $video_i$, we uniformly and independently sample two clips c_i, c'_i as a positive pair, while the clips in a batch belonging to other videos are used to construct negative pairs. The model processes clips c_i, c'_i to build respective vector representations f_i, f'_i and an InfoNCE [47] loss is used to distinguishes the positive feature pair (f_i, f'_i) from the negative pairs $\bigcup \{\{(f_i, f_k), (f_i, f'_k)\} \mid k \neq i\}$ for each clip c_i:

$$\mathcal{L}_{\text{InfoNCE}}(i) = -\log \frac{\exp\left(f_i^\top f'_i/\gamma\right)}{\sum_{k\neq i} \exp\left(f_i^\top f_k/\gamma\right) + \sum_k \exp\left(f_i^\top f'_k/\gamma\right)} \tag{4}$$

which we combine with the symmetric loss $\mathcal{L}'_{\text{InfoNCE}}(i)$ for paired clip sample c'_i. The final loss for a mini batch $\mathcal{L}_{\text{cl}}$ is the average loss for all n clips in the mini-batch:

$$\mathcal{L}_{\text{cl}} = \frac{1}{n}\sum_{i=1}^{n} \mathcal{L}_{\text{InfoNCE}}(i) + \frac{1}{n}\sum_{i=1}^{n} \mathcal{L}'_{\text{InfoNCE}}. \tag{5}$$

3.3. Pre-Training Objective

We combine the two pre-training methods discussed above to define the overall objective as:

$$\mathcal{L} = \mathcal{L}_{\text{mask}} + \alpha\gamma\mathcal{L}_{\text{cl}}, \tag{6}$$

where α is a hyperparameter controlling the weight of the contrastive loss and multiplying the temperature γ will smooth training [14, 29]. The inputs for both tasks are shared in mini-batches with the contrastive learning loss using the same block-masked inputs.

4. Experiments and Results

4.1. Datasets

For **pre-training**, we use the HowTo100M dataset [46]. HowTo100M has 1.2M uncurated videos, with an average duration of 6.5 minutes. For **downstream** evaluation, we experiment with several action classification datasets: UCF101 [56], HMDB51 [38], Kinetics-400 [10], SSV2 [28], and Diving48 [42]. It is important to note that in many cases, actions in UCF101, HMDB51, and Kinetics-400 can be recognized from a single frame of the video, thus these datasets are '*spatially-heavy*'. To test the video model's ability beyond recognizing static images, we lay our focus on '*temporally-heavy*' datasets (SSV2 and Diving48), in which action recognition from a single frame is more difficult. Additional dataset details (e.g., statistics) are presented in Appendix.

4.2. Results

Table 1 shows our primary results. We mainly compare with self-supervised pre-training methods on uncurated videos. In addition, we list methods with (weakly) supervised pre-training as references, though they can not be fairly compared with our method as they use large-scale

Table 1. **Comparison with state-of-the-art.** Our model outperforms previous works on SSV2 and Diving48 dataset while showing competitive results on other datasets. Results on UCF101 and HMDB51 are average over three train-val splits. V,A,T refer to Visual, Audio, and Text modalities, respectively. ^{a} [23,29], ^{b} [45], ^{c} [1], ^{d} [23,30], ^{e} [7], ^{f} [2], ^{g} [22], ^{h} [35], ^{j} [62], ^{k} [67], ^{l} [37]. K400=Kinetics-400 [10], HT=HowTo100M [46], AudioSet [25], IG-Uncurated [26], IN21K=ImageNet-21K [55]. Note that some SotA models are pre-trained with extremely large (weakly-)supervised datasets, e.g., IG65M [26] in ^{h} [35] and JFT-300M [60] in ^{f} [2].

Method	Modality	Pre-Train Dataset	Temporally-Heavy		Spatially-Heavy		
			SSV2	Diving48	UCF101	HMDB51	K400
(Weakly) Supervised Pre-Training							
K400 Sup.	V	K400	63.1^g	-	96.8^j	82.5^k	81.5^l
TimeSformer^e space-time	V	IN21K	62.3	81.0	-	-	80.7
TimeSformer^e space-only	V	IN21K	36.6	-	-	-	77.6
ViViT^f	V	IN21K/JFT300M	65.4	-	-	-	**84.8**
R(2+1)D BERT^h	V	IG65M	-	-	**98.7**	**85.1**	-
Self-supervised Pre-Training on Uncurated Videos							
MIL-NCE^b	V+T	HT	-	-	91.3	61.0	-
MMV^c	V+A+T	AudioSet + HT	-	-	95.2	75.0	-
BYOL^a	V	K400	55.8	-	96.3	75.0	-
MoCo^d	V	IG-Uncurated	53.2	-	92.9	-	-
VIMPAC	V	HT	**68.1**	**85.5**	92.7	65.9	75.3

(weakly) labeled data. As discussed in Sec. 4.1, recognizing actions in SSV2 and Diving48 require a strong temporal reasoning ability, while in the other datasets, spatial understanding is dominant. To better illustrate the differences between temporally-heavy and spatially-heavy datasets, we compare two variants of TimeSformer [7], one with attention on space-time, and one on space only. Note the gaps between these two variants are significantly larger for temporally-heavy datasets (SSV2) than spatially-heavy datasets (Kinetics-400), demonstrating the importance of temporal modeling for temporally-heavy datasets.[1] On the two temporally-heavy datasets SSV2 and Diving48, when comparing to previous best models among all self-supervised and supervised pre-training methods, our model VIMPAC sets new state of the art, where we achieve 2.7% and 4.5% absolute improvement, respectively. This is especially surprising considering the two previous SotA models ViViT [2] and TimeSformer [7] both use large-scale supervised pre-training, and ViViT also uses various regularization techniques (e.g., stochastic depth [32], random augment [16], and mixup [72]). On spatially-heavy datasets,UCF101, HMDB51 and Kinetics-400, VIMPAC achieves competitive results to self-supervised pre-training methods, while being lower when compared to supervised methods. These relatively low results of our VIMPAC (e.g., UCF101) are possibly due to the spatial information loss during the VQ-VQA quantization process. Concurrent work BEiT [4] addresses this issue by using image patches instead of VQ-VAE tokens as inputs, where they show strong performance on image classification tasks. We encourage future work to study using image patches as inputs for better spatial modeling under our framework. Previous self-supervised pre-training methods such as BYOL [23,29] and MoCo [23,30] are good at global understanding, but the pre-training schema does not consider the internal interactions inside videos (especially for the temporal dimension). As a result, it could reach or even outperform the supervised alternatives on UCF101. However, it shows lower results on SSV2 compared to the transformers [2, 7] (although with different backbones) that warm up from image-pre-trained models and learn the temporal interactions directly from the downstream tasks. We also show the cross-modal self-supervised learning methods, MIL-NCE [45] and MMV [1] that are trained on uncurated videos but leverage other modalities (e.g., text) to help video learning.

We provide the analysis results in Sec. F and Sec.G.

5. Conclusion

We present VIMPAC, a video self-supervised learning framework that introduces mask-then-predict task to help model spatio-temporal interactions that is important for video understanding. We use the VQ-VAE quantizer and propose the block masking method that is essential to overcome the strong locality in video. The contrastive learning task is also added to learn separable global features. Different from previous methods, our contrastive learning does not use data augmentation over raw frames and is less sensitive to the temporal sampling distribution for positive pairs. We show that our frameworks could achieve state-of-the-art performance on two temporally-heavy dataset (SSV2 and Diving48) and reach competitive results on other datasets. Detailed analysis is provided regarding the model scalability and task design.

[1]The image model CLIP [50] achieves 92.0% on the spatially-heavy UCF-101 dataset.

References

[1] Jean-Baptiste Alayrac, Adrià Recasens, Rosalia Schneider, Relja Arandjelović, Jason Ramapuram, Jeffrey De Fauw, Lucas Smaira, Sander Dieleman, and Andrew Zisserman. Self-supervised multimodal versatile networks. In *NeurIPS*, 2020. 4

[2] Anurag Arnab, Mostafa Dehghani, Georg Heigold, Chen Sun, Mario Lučić, and Cordelia Schmid. Vivit: A video vision transformer. *arXiv preprint arXiv:2103.15691*, 2021. 4, 7, 10, 13

[3] Jimmy Lei Ba, Jamie Ryan Kiros, and Geoffrey E Hinton. Layer normalization. In *NeurIPS*, 2016. 8, 9

[4] Hangbo Bao, Li Dong, and Furu Wei. Beit: Bert pre-training of image transformers. *arXiv preprint arXiv:2106.08254*, 2021. 2, 4, 17

[5] Sagie Benaim, Ariel Ephrat, Oran Lang, Inbar Mosseri, William T Freeman, Michael Rubinstein, Michal Irani, and Tali Dekel. Speednet: Learning the speediness in videos. In *Proceedings of the IEEE/CVF Conference on Computer Vision and Pattern Recognition*, pages 9922–9931, 2020. 2

[6] Marcelo Bertalmio, Andrea L Bertozzi, and Guillermo Sapiro. Navier-stokes, fluid dynamics, and image and video inpainting. In *Proceedings of the 2001 IEEE Computer Society Conference on Computer Vision and Pattern Recognition. CVPR 2001*, volume 1, pages I–I. IEEE, 2001. 2

[7] Gedas Bertasius, Heng Wang, and Lorenzo Torresani. Is space-time attention all you need for video understanding? In *ICML*, 2021. 4, 7, 8, 10, 12, 13, 14, 15

[8] Mathilde Caron, Ishan Misra, Julien Mairal, Priya Goyal, Piotr Bojanowski, and Armand Joulin. Unsupervised learning of visual features by contrasting cluster assignments. *arXiv preprint arXiv:2006.09882*, 2020. 2

[9] Joao Carreira, Eric Noland, Chloe Hillier, and Andrew Zisserman. A short note on the kinetics-700 human action dataset. *arXiv preprint arXiv:1907.06987*, 2019. 11

[10] Joao Carreira and Andrew Zisserman. Quo vadis, action recognition? a new model and the kinetics dataset. In *proceedings of the IEEE Conference on Computer Vision and Pattern Recognition*, pages 6299–6308, 2017. 1, 3, 4, 16

[11] Mark Chen, Alec Radford, Rewon Child, Jeffrey Wu, Heewoo Jun, David Luan, and Ilya Sutskever. Generative pretraining from pixels. In *International Conference on Machine Learning*, pages 1691–1703. PMLR, 2020. 2, 10

[12] Ting Chen, Simon Kornblith, Mohammad Norouzi, and Geoffrey Hinton. A simple framework for contrastive learning of visual representations. *arXiv preprint arXiv:2002.05709*, 2020. 1, 2, 12, 13

[13] Xinlei Chen, Haoqi Fan, Ross Girshick, and Kaiming He. Improved baselines with momentum contrastive learning. *arXiv preprint arXiv:2003.04297*, 2020. 1, 2, 13

[14] Xinlei Chen, Saining Xie, and Kaiming He. An empirical study of training self-supervised visual transformers. *arXiv e-prints*, pages arXiv–2104, 2021. 3, 7, 9, 10, 13

[15] Rewon Child, Scott Gray, Alec Radford, and Ilya Sutskever. Generating long sequences with sparse transformers. *arXiv preprint arXiv:1904.10509*, 2019. 7, 8, 9, 10, 14

[16] Ekin D Cubuk, Barret Zoph, Jonathon Shlens, and Quoc V Le. Randaugment: Practical automated data augmentation with a reduced search space. In *Proceedings of the IEEE/CVF Conference on Computer Vision and Pattern Recognition Workshops*, pages 702–703, 2020. 4

[17] Jacob Devlin, Ming-Wei Chang, Kenton Lee, and Kristina Toutanova. Bert: Pre-training of deep bidirectional transformers for language understanding. In *Proceedings of the 2019 Conference of the North American Chapter of the Association for Computational Linguistics: Human Language Technologies, Volume 1 (Long and Short Papers)*, pages 4171–4186, 2019. 1, 2, 7, 8, 9, 10

[18] Carl Doersch, Abhinav Gupta, and Alexei A Efros. Unsupervised visual representation learning by context prediction. In *Proceedings of the IEEE international conference on computer vision*, pages 1422–1430, 2015. 2

[19] Alexey Dosovitskiy, Lucas Beyer, Alexander Kolesnikov, Dirk Weissenborn, Xiaohua Zhai, Thomas Unterthiner, Mostafa Dehghani, Matthias Minderer, Georg Heigold, Sylvain Gelly, et al. An image is worth 16x16 words: Transformers for image recognition at scale. In *ICLR*, 2021. 8, 9, 12

[20] Dave Epstein, Boyuan Chen, and Carl Vondrick. Oops! predicting unintentional action in video. In *Proceedings of the IEEE/CVF conference on computer vision and pattern recognition*, pages 919–929, 2020. 2

[21] Patrick Esser, Robin Rombach, and Bjorn Ommer. Taming transformers for high-resolution image synthesis. In *Proceedings of the IEEE/CVF Conference on Computer Vision and Pattern Recognition*, pages 12873–12883, 2021. 17

[22] Christoph Feichtenhofer, Haoqi Fan, Jitendra Malik, and Kaiming He. Slowfast networks for video recognition. In *Proceedings of the IEEE/CVF International Conference on Computer Vision*, pages 6202–6211, 2019. 4, 10, 12

[23] Christoph Feichtenhofer, Haoqi Fan, Bo Xiong, Ross Girshick, and Kaiming He. A large-scale study on unsupervised spatiotemporal representation learning. *arXiv preprint arXiv:2104.14558*, 2021. 2, 4, 10, 13

[24] Basura Fernando, Hakan Bilen, Efstratios Gavves, and Stephen Gould. Self-supervised video representation learning with odd-one-out networks. In *Proceedings of the IEEE conference on computer vision and pattern recognition*, pages 3636–3645, 2017. 2

[25] Jort F Gemmeke, Daniel PW Ellis, Dylan Freedman, Aren Jansen, Wade Lawrence, R Channing Moore, Manoj Plakal, and Marvin Ritter. Audio set: An ontology and human-labeled dataset for audio events. In *2017 IEEE International Conference on Acoustics, Speech and Signal Processing (ICASSP)*, pages 776–780. IEEE, 2017. 4

[26] Deepti Ghadiyaram, Du Tran, and Dhruv Mahajan. Large-scale weakly-supervised pre-training for video action recognition. In *Proceedings of the IEEE/CVF Conference on Computer Vision and Pattern Recognition*, pages 12046–12055, 2019. 4

[27] Spyros Gidaris, Praveer Singh, and Nikos Komodakis. Unsupervised representation learning by predicting image rotations. *arXiv preprint arXiv:1803.07728*, 2018. 2

[28] Raghav Goyal, Samira Ebrahimi Kahou, Vincent Michalski, Joanna Materzyńska, Susanne Westphal, Heuna Kim, Valentin Haenel, Ingo Fruend, Peter Yianilos, Moritz Mueller-Freitag, Florian Hoppe, Christian Thurau, Ingo Bax, and Roland Memisevic. The ”something something” video database for learning and evaluating visual common sense, 2017. 3, 16

[29] Jean-Bastien Grill, Florian Strub, Florent Altché, Corentin Tallec, Pierre H Richemond, Elena Buchatskaya, Carl Doersch, Bernardo Avila Pires, Zhaohan Daniel Guo, Mohammad Gheshlaghi Azar, et al. Bootstrap your own latent a new approach to self-supervised learning. In *NeurIPS*, 2020. 2, 3, 4, 13

[30] Kaiming He, Haoqi Fan, Yuxin Wu, Saining Xie, and Ross Girshick. Momentum contrast for unsupervised visual representation learning. In *Proceedings of the IEEE/CVF Conference on Computer Vision and Pattern Recognition*, pages 9729–9738, 2020. 1, 2, 4

[31] Dan Hendrycks and Kevin Gimpel. Gaussian error linear units (gelus). *arXiv preprint arXiv:1606.08415*, 2016. 8, 9

[32] Gao Huang, Yu Sun, Zhuang Liu, Daniel Sedra, and Kilian Q Weinberger. Deep networks with stochastic depth. In *European conference on computer vision*, pages 646–661. Springer, 2016. 4

[33] Sergey Ioffe and Christian Szegedy. Batch normalization: Accelerating deep network training by reducing internal covariate shift. In *International conference on machine learning*, pages 448–456. PMLR, 2015. 9

[34] Mandar Joshi, Danqi Chen, Yinhan Liu, Daniel S Weld, Luke Zettlemoyer, and Omer Levy. Spanbert: Improving pretraining by representing and predicting spans. *Transactions of the Association for Computational Linguistics*, 8:64–77, 2020. 2

[35] M Esat Kalfaoglu, Sinan Kalkan, and A Aydin Alatan. Late temporal modeling in 3d cnn architectures with bert for action recognition. In *European Conference on Computer Vision*, pages 731–747. Springer, 2020. 4

[36] Dahun Kim, Sanghyun Woo, Joon-Young Lee, and In So Kweon. Deep video inpainting. In *Proceedings of the IEEE/CVF Conference on Computer Vision and Pattern Recognition*, pages 5792–5801, 2019. 2

[37] Dan Kondratyuk, Liangzhe Yuan, Yandong Li, Li Zhang, Mingxing Tan, Matthew Brown, and Boqing Gong. Movinets: Mobile video networks for efficient video recognition. *arXiv preprint arXiv:2103.11511*, 2021. 4

[38] Hilde Kuehne, Hueihan Jhuang, E. Garrote, T. Poggio, and Thomas Serre. Hmdb: A large video database for human motion recognition. *2011 International Conference on Computer Vision*, pages 2556–2563, 2011. 3

[39] Hildegard Kuehne, Hueihan Jhuang, Estíbaliz Garrote, Tomaso Poggio, and Thomas Serre. Hmdb: a large video database for human motion recognition. In *2011 International conference on computer vision*, pages 2556–2563. IEEE, 2011. 16

[40] Zhenzhong Lan, Mingda Chen, Sebastian Goodman, Kevin Gimpel, Piyush Sharma, and Radu Soricut. Albert: A lite bert for self-supervised learning of language representations. In *International Conference on Learning Representations*, 2019. 1, 2

[41] Hsin-Ying Lee, Jia-Bin Huang, Maneesh Singh, and Ming-Hsuan Yang. Unsupervised representation learning by sorting sequences. In *Proceedings of the IEEE International Conference on Computer Vision*, pages 667–676, 2017. 2

[42] Yingwei Li, Yi Li, and Nuno Vasconcelos. Resound: Towards action recognition without representation bias. In *Proceedings of the European Conference on Computer Vision (ECCV)*, pages 513–528, 2018. 3, 16

[43] Yinhan Liu, Myle Ott, Naman Goyal, Jingfei Du, Mandar Joshi, Danqi Chen, Omer Levy, Mike Lewis, Luke Zettlemoyer, and Veselin Stoyanov. Roberta: A robustly optimized bert pretraining approach. *arXiv preprint arXiv:1907.11692*, 2019. 1

[44] Ilya Loshchilov and Frank Hutter. Decoupled weight decay regularization. In *International Conference on Learning Representations*, 2018. 10

[45] Antoine Miech, Jean-Baptiste Alayrac, Lucas Smaira, Ivan Laptev, Josef Sivic, and Andrew Zisserman. End-to-end learning of visual representations from uncurated instructional videos. In *Proceedings of the IEEE/CVF Conference on Computer Vision and Pattern Recognition*, pages 9879–9889, 2020. 4

[46] Antoine Miech, Dimitri Zhukov, Jean-Baptiste Alayrac, Makarand Tapaswi, Ivan Laptev, and Josef Sivic. HowTo100M: Learning a Text-Video Embedding by Watching Hundred Million Narrated Video Clips. In *ICCV*, 2019. 3, 4, 11

[47] Aaron van den Oord, Yazhe Li, and Oriol Vinyals. Representation learning with contrastive predictive coding. *arXiv preprint arXiv:1807.03748*, 2018. 1, 3

[48] Ofir Press and Lior Wolf. Using the output embedding to improve language models. In *Proceedings of the 15th Conference of the European Chapter of the Association for Computational Linguistics: Volume 2, Short Papers*, pages 157–163, 2017. 9

[49] Rui Qian, Tianjian Meng, Boqing Gong, Ming-Hsuan Yang, Huisheng Wang, Serge Belongie, and Yin Cui. Spatiotemporal contrastive video representation learning. In *CVPR*, 2021. 10, 12, 13

[50] Alec Radford, Jong Wook Kim, Chris Hallacy, Aditya Ramesh, Gabriel Goh, Sandhini Agarwal, Girish Sastry, Amanda Askell, Pamela Mishkin, Jack Clark, et al. Learning transferable visual models from natural language supervision. *arXiv preprint arXiv:2103.00020*, 2021. 4

[51] Colin Raffel, Noam Shazeer, Adam Roberts, Katherine Lee, Sharan Narang, Michael Matena, Yanqi Zhou, Wei Li, and Peter J Liu. Exploring the limits of transfer learning with a unified text-to-text transformer. *arXiv preprint arXiv:1910.10683*, 2019. 2

[52] Aditya Ramesh, Mikhail Pavlov, Gabriel Goh, Scott Gray, Chelsea Voss, Alec Radford, Mark Chen, and Ilya Sutskever. Zero-shot text-to-image generation. *arXiv preprint arXiv:2102.12092*, 2021. 2, 7, 9, 10, 13, 17

[53] Ali Razavi, Aäron van den Oord, and Oriol Vinyals. Generating diverse high-fidelity images with vq-vae-2. In *NeurIPS*, 2019. 2

[54] Sebastian Ruder, Matthew E. Peters, Swabha Swayamdipta, and Thomas Wolf. Transfer learning in natural language processing. In *Proceedings of the 2019 Conference of the North American Chapter of the Association for Computational Linguistics: Tutorials*, pages 15–18, Minneapolis, Minnesota, June 2019. Association for Computational Linguistics. 2

[55] Olga Russakovsky, Jia Deng, Hao Su, Jonathan Krause, Sanjeev Satheesh, Sean Ma, Zhiheng Huang, Andrej Karpathy, Aditya Khosla, Michael Bernstein, et al. Imagenet large scale visual recognition challenge. *International journal of computer vision*, 115(3):211–252, 2015. 4, 12

[56] K. Soomro, A. Zamir, and M. Shah. Ucf101: A dataset of 101 human actions classes from videos in the wild. *ArXiv*, abs/1212.0402, 2012. 3

[57] Khurram Soomro, Amir Roshan Zamir, and Mubarak Shah. Ucf101: A dataset of 101 human actions classes from videos in the wild. *arXiv preprint arXiv:1212.0402*, 2012. 1, 16

[58] Chen Sun, Austin Myers, Carl Vondrick, Kevin Murphy, and Cordelia Schmid. Videobert: A joint model for video and language representation learning. In *Proceedings of the IEEE/CVF International Conference on Computer Vision*, pages 7464–7473, 2019. 2

[59] Chen Sun, Arsha Nagrani, Yonglong Tian, and Cordelia Schmid. Composable augmentation encoding for video representation learning. *arXiv preprint arXiv:2104.00616*, 2021. 2

[60] Chen Sun, Abhinav Shrivastava, Saurabh Singh, and Abhinav Gupta. Revisiting unreasonable effectiveness of data in deep learning era. In *Proceedings of the IEEE international conference on computer vision*, pages 843–852, 2017. 4, 12

[61] Yonglong Tian, Chen Sun, Ben Poole, Dilip Krishnan, Cordelia Schmid, and Phillip Isola. What makes for good views for contrastive learning. *arXiv preprint arXiv:2005.10243*, 2020. 1

[62] Du Tran, Heng Wang, Lorenzo Torresani, Jamie Ray, Yann LeCun, and Manohar Paluri. A closer look at spatiotemporal convolutions for action recognition. In *Proceedings of the IEEE conference on Computer Vision and Pattern Recognition*, pages 6450–6459, 2018. 4

[63] Aäron van den Oord, Nal Kalchbrenner, Lasse Espeholt, K. Kavukcuoglu, Oriol Vinyals, and A. Graves. Conditional image generation with pixelcnn decoders. In *NIPS*, 2016. 2

[64] Aäron van den Oord, Oriol Vinyals, and Koray Kavukcuoglu. Neural discrete representation learning. In *NeurIPS*, 2017. 2, 7, 9

[65] Ashish Vaswani, Noam Shazeer, Niki Parmar, Jakob Uszkoreit, Llion Jones, Aidan N Gomez, Łukasz Kaiser, and Illia Polosukhin. Attention is all you need. In *Advances in neural information processing systems*, pages 5998–6008, 2017. 8

[66] Jacob Walker, Ali Razavi, and Aäron van den Oord. Predicting video with vqvae. *arXiv preprint arXiv:2103.01950*, 2021. 2, 7

[67] Lei Wang, Piotr Koniusz, and Du Q Huynh. Hallucinating idt descriptors and i3d optical flow features for action recognition with cnns. In *Proceedings of the IEEE/CVF International Conference on Computer Vision*, pages 8698–8708, 2019. 4

[68] Donglai Wei, Joseph J Lim, Andrew Zisserman, and William T Freeman. Learning and using the arrow of time. In *Proceedings of the IEEE Conference on Computer Vision and Pattern Recognition*, pages 8052–8060, 2018. 2

[69] Wilson Yan, Yunzhi Zhang, Pieter Abbeel, and Aravind Srinivas. Videogpt: Video generation using vq-vae and transformers. *arXiv preprint arXiv:2104.10157*, 2021. 2

[70] Zhilin Yang, Zihang Dai, Yiming Yang, Jaime Carbonell, Russ R Salakhutdinov, and Quoc V Le. Xlnet: Generalized autoregressive pretraining for language understanding. In *Advances in neural information processing systems*, pages 5754–5764, 2019. 1

[71] Jiahui Yu, Zhe Lin, Jimei Yang, Xiaohui Shen, Xin Lu, and Thomas S Huang. Generative image inpainting with contextual attention. In *Proceedings of the IEEE conference on computer vision and pattern recognition*, pages 5505–5514, 2018. 2

[72] Hongyi Zhang, Moustapha Cisse, Yann N Dauphin, and David Lopez-Paz. mixup: Beyond empirical risk minimization. In *International Conference on Learning Representations*, 2018. 4

[73] Richard Zhang, Phillip Isola, and Alexei A Efros. Colorful image colorization. In *European conference on computer vision*, pages 649–666. Springer, 2016. 2

In this supplementary materials, we start with describing details of the model (Sec. A), pre-training (Sec. B), experiments (Sec. C), and dataset (Sec. D). We then provide additional analysis results in Sec. G and visualization in Sec. H.

A. Model Architecture

We use a transformer model on top of the discrete video tokens generated by VQ-VAE. Since transformers have different variants, we here show details of our architecture for clarity. The design of our method largely follows the practice in BERT [17], TimeSformer [7], Sparser Transformer [15], ViViT [2], and MoCoV3 [14].

A.1. Backbone Model

Embedding. Given the video frames $\{f_t \in \mathbb{R}^{H\times W} \mid t \in [T]\}$, we first use VQ-VAE [52, 64] to discrete them into video tokens $\{x_{t,i,j} \in [V] \mid t \in [\hat{T}], i \in [\hat{H}], j \in [\hat{W}]\}$. We use the specific VQ-VAE in DALL-E [52] which is trained on trained on 250 million images from the Internet. [2] Since the VQ-VAE encoder largely compresses a 8x8x3 vector (ranging from 0-255) to an integer of 0-8191, it is considered as a compression method with image prior. We do not use the Video-VQVAE [66] method since the image-trained VQVAE has been pretrained on a very large image corpus and as a consequence cover a much more diverse set of visual scenes and elements. We next use an embedding layer

[2]The VQ-VAE compression method is trained on 250M images as in [52]. However, the VQ-VAE does not help with a better representation for the video pre-training as shown in Sec. F.2.1, where directly training on the VQ-VAE tokens provides poor results.

($embedding$) that to map these discrete tokens to continuous vectors. Since transformer layers are permutation-invariant, we follow [17, 19] to add positional information into the input. The positional embedding (pos) is factorized as a sum of the temporal embedding pos^{T}, the height embedding pos^{H}, and the width embedding pos^{W}. This factorization reduces the number of trainable parameters to encode positional information, which empirically shows a slightly better result. Finally, a Layer-Normalization [3] layer is added to get the initial hidden outputs $h^0_{t,i,j}$:

$$h^0_{t,i,j} = \mathrm{LayerNorm}(embed(x_{t,i,j}) + pos(t,i,j)), \tag{7}$$

$$pos(t,i,j) = pos^{\mathrm{T}}(t) + pos^{\mathrm{H}}(i) + pos^{\mathrm{W}}(j), \tag{8}$$

where we use the superscript 0 to denote that it is the hidden outputs before the first transformer layer.

Attention Blocks. Before introducing the detailed model architecture, we first describe the basic building components: the attention block. An attention block is built based on the attention operator (i.e., 'Attn') with a residual connection. The attention operator takes a single query vector x and its context $\{y_i\}$ as input. It first computes the attention score between x and each context vector y_i, then the attention scores are normalized by the $\mathrm{softmax}$. Lastly, the output is a weighted-sum over all the context vectors (transferred by a 'value' matrix W_{value}):

$$\mathrm{Attn}(x, \{y_i\}) = \sum_i \mathrm{softmax}_i\{(W_{\text{query}}\, x)^\top W_{\text{key}}\, y_i\} W_{\text{value}}\, y_i. \tag{9}$$

To compose the attention block from the previous attention operator, the residual connection and layer normalization (i.e., 'LN') are added. We follow the original transformer model [65] that uses a post-layer-norm layout:

$$\mathrm{AttnBlock}(x, \{y_i\}) = \mathrm{LN}(x + W_{\text{out}}\, \mathrm{Attn}(x, \{y_i\})). \tag{10}$$

In order to reduce computational cost and memory, we also adapt the attention block suggested in Sparse Transformer [15] that takes two sets of context vectors $\{y_i\}$ and $\{z_j\}$ as input. This special attention block computes attention for the two context-vector sets separately and concatenates their output together. In our case, suppose $\{y_i\}$ and $\{z_j\}$ are the rows and columns of a square matrix, then it reduces the computation cost of calculating attention scores from $\Theta(n^4)$ to $\Theta(n^2)$, where n is the number of rows/columns:

$$\begin{aligned}\mathrm{AttnBlock}(x, \{y_i\}, \{z_j\}) = \mathrm{LN}(&x \\ &+ W_{\text{out}}\, [\mathrm{Attn}(x, \{y_i\}), \mathrm{Attn}(x, \{z_j\})])\end{aligned} \tag{11}$$

Spatio-Temporal Transformer Layer. The spatio-temporal transformer layer is composed with the previously-introduced attention blocks and an additional MLP block. The l-th layer takes the output of the previous layer $\{h^{l-1}_{t,i,j}\}$ as input and outputs the hidden states $\{h^l_{t,i,j}\}$. We separate the attention into two attention blocks: the temporal attention block $\mathrm{AttnBlock}_{\text{TIME}}$ and the spatial attention block $\mathrm{AttnBlock}_{\text{SPACE}}$. Without loss of generality, we will use g^{TIME} and g^{SPACE} to denote the intermediate results from temporal and spatial attention blocks, respectively. First, the temporal attention block attends to the tokens at the same spatial location but in different frames (i.e., at different timesteps): $\{h^{l-1}_{t,i,j} \mid t \in [T]\}$. Next, the spatial attention block attends to the tokens in the same frame: $\{g^{\mathrm{T}}_{t,i,j} \mid (i,j) \in [\hat{H}] \times [\hat{W}]\}$. To reduce the computational cost, we incorporate the sparse attention block [15] (detailed in the previous paragraph) that factorizes the attention over height and width: $\{g^{\mathrm{T}}_{t,i,j} \mid i \in [\hat{H}]\}$, $\{g^{\mathrm{T}}_{t,i,j} \mid j \in [\hat{W}]\}$. The MLP block has two fully-connected layers with GeLU [31] activation in the middle. Overall, the formula of one spatio-temporal transformer layer is:

$$g^{\text{TIME}}_{t,i,j} = \mathrm{AttnBlock}_{\text{TIME}}(h^{l-1}_{t,i,j}, \{h^{l-1}_{t,i,j} \mid t \in [T]\}) \tag{12}$$

$$\begin{aligned}g^{\text{SPACE}}_{t,i,j} = \mathrm{AttnBlock}_{\text{SPACE}}(&\\ &g^{\mathrm{T}}_{t,i,j}, \{g^{\text{TIME}}_{t,i,j} \mid i \in [\hat{H}]\}, \{g^{\text{TIME}}_{t,i,j} \mid j \in [\hat{W}]\})\end{aligned} \tag{13}$$

$$h^l_{t,i,j} = \mathrm{LayerNorm}(g^{\text{SPACE}}_{t,i,j} + \mathrm{MLP}(g^{\mathrm{S}}_{t,i,j})) \tag{14}$$

`[CLS]` Token. Following the practice in BERT [17] design, we add a special `[CLS]` (abbreviation of 'classification') token and take its output as the representation of the whole sequence. We follow TimeSformer [7] to compute the its output: the `[CLS]` token attends over the context separately and then the outputs are averaged. We take the temporal attention layer as an example. Suppose h^{l-1}_{cls} is the `[CLS]` feature vector output by layer $l-1$, then the temporal attention layer do the following computation:

$$g^{\text{TIME}}_{\text{cls}} = \frac{1}{\hat{H}} \frac{1}{\hat{W}} \sum_i \sum_j \mathrm{AttnBlock}_{\text{TIME}}(h^{l-1}_{\text{cls}}, \{h^{l-1}_{t,i,j} \mid t \in [T]\}). \tag{15}$$

The other attention blocks process the `[CLS]` token similarly.

A.2. Pre-Training and Fine-Tuning Heads

Pre-training or fine-tuning usually requires a few additional modules (i.e., heads) on top of the transformer layers that convert the output features to the desired probabilities or vectors. We next describe the heads used in our pre-training and fine-tuning process.

Token Head for Mask-then-Predict. We first define the prediction head over the tokens following BERT [17]. It first processes the last-layer hidden outputs $h^L_{t,i,j}$ using a fully-connected layer (with GELU activation [31] and layer normalization [3]):

$$u_{t,i,j} = \mathrm{LayerNorm}\left(\mathrm{GELU}(W_{\text{token}}(h^L_{t,i,j}) + b_{\text{token}})\right). \tag{16}$$

In our mask-then-predict method (Sec. 3.1), we will predict the masked tokens (i.e., the token before masking) from their context. We thus further convert this hidden vector into a distribution over the token vocabulary:

$$P_{t,i,j}(o_{t,i,j} = k) = \mathrm{softmax}_k\{W_{\text{word}}\, u_{t,i,j} + b_{\text{word}}\}. \tag{17}$$

The weight W_{word} is shared with input word embedding layer *embedding* [17, 48] while the bias b_{word} is trained independently.

Contrastive Learning Head Next we discuss the pre-training heads for contrastive learning. It is on top of the `[CLS]` hidden output h_{CLS}. We encode the hidden state with MLP. We use batch normalization [33] inside the MLP head following the practice in [14].

$$f_{\text{CLS}} = \mathrm{MLP}_{\text{CLS}}(h_{\text{CLS}}) \tag{18}$$

This f_{CLS} feature is used in computing the contrastive loss as in Sec. 3.2.

FC Layer for Fine-Tuning. When fine-tuning for action classification task, we add a fully-connected (FC) layer to the `[CLS]` output h_{cls}. We initialize its weight and bias to zero.

Special Tokens. Besides the V token types introduced in the vocabulary of the VQ-VAE (see Sec. 3.1), we add several special tokens into the 'vocabulary', namely a `[CLS]` token is introduced as a stub for the whole-video representation, a `[PAD]` token is used when the actual clip length is less than the model's expected input length. For the mask-then-predict task, we follow BERT [17] to replace the masked tokens with a specific `[MASK]` token.

B. Pre-Training Details

B.1. Masking Blocks

As described in Sec. 3.1, we mask the tokens by blocks (a cube-shape set of tokens). To avoid masking all the tokens in the clip, we control the maximum block length for the time domain, height, and width. For spatial dimensions (i.e., height and width), the maximum length is half of the full length (e.g., the maximum block length will be 16 for a token map of length 32). For temporal dimension (i.e., the clip length), the maximum length will be 2/3 (round up) of the full length so that it allows long-range modeling. Under these constraints, we uniformly sample a fixed number of mask blocks and take their union to construct the final mask. The number of blocks is decided by the induced masking ratio, which depends on the input resolutions. In Table 2, we show the induced masking ratio w.r.t. different input resolutions and #masking blocks. We take the VQ-VAE [64] provided in DALL-E [52] that has a compression factor of 8, thus the length of the token map is always 1/8 of the frame size. For each input resolution, we select the number of blocks (shown in bold in Table 2) whose induced masking ratio is closet to 15% following BERT [17].

B.2. Contrastive Learning Loss

For completeness, we list the two losses used in contrastive learning here. The first loss for clip c_i from video$_i$ is:

$$\mathcal{L}_{\text{InfoNCE}}(i) = -\log \frac{\exp\left(f_i^\top f'_i/\gamma\right)}{\sum_{k\neq i}\exp\left(f_i^\top f_k/\gamma\right) + \sum_k \exp\left(f_i^\top f'_k/\gamma\right)} \tag{19}$$

The symmetric loss $\mathcal{L}'_{\text{InfoNCE}}(i)$ for feature of the other clip sample c'_i from video$_i$ (and its feature f'_i) is:

$$\mathcal{L}'_{\text{InfoNCE}}(i) = -\log \frac{\exp\left(f'^\top_i f_i/\gamma\right)}{\sum_k \exp\left(f'^\top_i f_k/\gamma\right) + \sum_{k\neq i}\exp\left(f'^\top_i f'_k/\gamma\right)} \tag{20}$$

C. Experiment Details

In this section, we show our model configuration and training hyperparameters in details to support the reproducibility of our experiments.

C.1. Experimental Setup

Our model shapes follow BERT$_{\text{LARGE}}$ with 24 layers and hidden size 1024, but with halved attention head size and MLP intermediate size as in [15]. For **pre-training**, we train the model for 100 epochs on HowTo100M with frames sampled at 2 FPS. We sample two clips from each video as model inputs as described in Sec. 3.2. Positional embeddings are interpolated as in [19] when input resolution changes. Importantly, our pre-training scheme does not involve spatial augmentations: all frames are resized and centered cropped without random flipping, color distortion, etc. We use a batch size of 1024 in pre-training. The number of negative clips used for contrastive learning is 255 for the first 90 epochs and 127 for the last 10 epochs. The number of negative pairs used in our ablation analyses is kept constant at 127. More details are in Appendix. For **fine-tuning**, we use more input frames (T=10 and S=256), and

Table 2. **Induced Masking ratio** w.r.t. to different input resolutions and #masking blocks. The numbers of blocks/masking ratio for each resolution setting used in our experiments are shown in **bold**.

Input Resolution			#Masking Blocks				
Length	Frame Size	Token Map Size	4	5	6	7	8
5	128	16	11.9	**14.5**	17.0	19.4	21.7
5	256	32	10.6	13.1	**15.2**	17.5	19.5
10	128	16	10.4	12.8	**15.0**	17.1	19.2
10	256	32	9.3	11.4	13.4	**15.4**	17.2

Table 3. **Model Configuration**. The 'Small' model is mainly used in the analysis (Sec. F) while 'Large-Half' model is mainly used in the results (Sec. 4.2) for the final large-scale experiments. 'Vocab Size' is the number of token types in our model, defined by the pre-trained VQ-VAE model [52].

	Small (in Sec. F)	Base	Large-Half (in Sec. 4.2)
Layers	6	12	24
Dimensions	512	768	1024
Attention Heads	8	12	16
Attention Head Dim	64	64	32
MLP Intermediate Size	2048	3072	2048
Vocab Size	8192	8192	8192
Params	29.4M	119.7M	210.1M

batch size 128. We sample frames at 2 FPS for datasets with longer videos (i.e., UCF101 and Kinetics-400), and sample 4 FPS for datasets with shorter videos (i.e., HMDB51, SSV2, Diving48). During inference, we follow [22, 23] to use 3 spatial crops and 10 temporal crops (in total 30 crops), and average their prediction scores as the final score.[3] All models are trained with AdamW [44] optimizer with linear warm-up and linear learning rate decay. We observe similar pre-training instability as reported in [11, 14] and follow their practice to sequentially choose learning rate at 1e-3, 5e-4, 3e-4, ..., until convergence.

Model Configuration. Our model configuration details is shown in Table 3. Most analysis results (Sec. F) take 'Small' models and our final results (Sec. 4.2) take 'Large-Half' model. Other models are used in Sec. F.1. The final 'Large-Half' model halves the attention head dimension and MLP intermediate size as in [15]. For the pre-training heads, we follow BERT to take the intermediate dimension of the token-head to be the same as the backbone's hidden dimension. For the CLS head, we take 3 layers in MLP and 4096 intermediate dimensions. The output dimension is 256. We test with different number of layers and hidden dimensions of CLS head and generally find that larger head gives better results (as in [14, 49]). This CLS head contributes to about 1% pre-training computational cost overhead.

Training Hyperparameters. We list the training hyperparameters in Table 4. Most of the hyperparameters are inherited from previous works to allow fair comparison and reduce tuning effort. For optimizer hyperparameters, we mostly follow the implementation of DALL-E [52] and BERT [17]. SSV2 follows the epoch number in [22] and [23]. To reduce the computational cost, we pre-extract the VQ-VAE tokens thus we employ a fixed set of spatial data augmentations. As listed in the bottom of Table 4, we exclude any color distortion and gray scale augmentation. We resize the video clip to the desired frame size and center-crop it during pre-training. For downstream tasks, we resize the video clip to frame size or 1.5 times of the frame size, then crop the clip (with frame-size by frame-size spatial size) from the top-left, center, and bottom-right. We apply (horizontal) flip to the raw frames thus a total of 12 spatial augmentations are extracted (12 = 2 resize $\times$ 3 crops $\times$ 3 flip/no-flip). The only exception is SSV2. This dataset needs to distinguish left/right motions thus we exclude the flip augmentation and only use the center crop during inference following previous works [22, 23]. During pre-training, we always accumulate the gradient to a batch size of 1024 before updating the weights but use different numbers of negative examples. We analyze this effect in Sec. F.2.3.

Following previous works [22], we increase the training epochs for the non-pre-training models by 4$\times$ for

[3] As in [2, 7], we observe that the performance is saturated at 4$\sim$5 temporal crops for our model.

Table 4. **Training Hyperparameters**. 'Pre-Train (Results)' is our final model in Sec. 4.2 that takes a large-half model. 'Pre-Train (Analysis)' is the pre-training in analysis (Sec. F). *The batch size for pre-training is the number of samples in updating the weights, Since we use gradient accumulation, it is not correlated to the number of negative examples in contrastive learning.

	Pre-Train (Results)	Pre-Train (Analysis)	SSV2	Diving48	UCF101	HMDB51	Kinetics-400
Optimization							
Number of Epochs	100	10	22	50	50	50	30
Number of Updates	120K	12K	29K	5.8K	3.7K	1.4K	48K
Learning Rate	3e-4	1e-3	1e-4 for small/base model, 5e-5 for large-half model				
Warm-Up Ratio	0.05	0.1	0.1				
LR Decay	Linear		Linear				
Backbone Dropout	0.1		0.1				
Last FC Dropout	-		0.0				
Optimizer	AdamW		AdamW				
Batch Size	1024*		128				
Weight-Decay	0.05		0.01				
Adam Beta1	0.9		0.9				
Adam Beta2	0.98		0.999				
Adam Epsilon	1e-8		1e-8				
Grad-Clipping Norm	1.0		1.0				
Data Augmentation							
Color Distortion/Gray-Scale	No		No				
Training Spatial Resize	1 (Frame Size)		2 (Frame Size, Frame Size * 1.25)				
Training Spatial Crops	1 (Center)		3 (Top-Left, Center, Bottom-Right)				
Training Temporal Crops	2 (Random Uniform)		1 (Random Uniform)				
Inference Spatial Resize	1 (Frame Size)		1 (Frame Size)				
Inference Temporal Crops	1 (Random Uniform)		10 (Uniform)				
Training Spatial Flip	No		No	Yes			
Inference Spatial Crops	1 (Center)		1 (Center)	3 (Top-Left, Center, Bottom-Right)			

small datasets (Diving48, UCF101, HMDB51) and 1.5× for larger datasets (SSV2, Kinetics-400).

When analyzing the mask-then-predict task in Sec. F.2.2 (and all other analysis focusing on mask-then-predict), we exclude the contrastive learning loss (by setting loss weight α=0) to preclude potential side effects. However, we still use masked prediction loss when assessing the contrastive learning task in Sec. F.2.3 as we observe very low performance with only contrastive learning objective.

Pre-Training with Kinetics datasets. Besides pre-training on the HowTo100M [46] dataset, we have an experiment with smaller models (i.e., base model in Table 3) pre-trained on K600 dataset. We found that the pure mask-prediction task on K600 [9] can reach 88% on UCF101, but adding the contrastive learning task does not show significant further improvement (+0.5%$\sim$1% according to the hyperparameters and seeds). This is possibly due to K600 dataset is designed specifically for action recognition on shorter video-clip where the average length of the video is 10 second. This short-range video would limit the success of the masked prediction and contrastive learning combination (as illustrated in Table 10 on HowTo100M dataset, d_{max} = 10s). Given these observations, we did not run the full model (large model in Table 3) on K600 because of the budget constraint.

D. Dataset Details

In Table 5, we list the key statistics of the datasets used in our paper. HowTo100M is our pre-training datasets that has long-duration uncurated videos. The videos are collected from YouTube by searching key phrases thus the scale could be easily increased. SSV2 and Kinetics-400 are two large downstream datasets, where SSV2 focuses more on the actions and Kinetics-400 focuses more on the scenes. Diving48, UCF101, HMDB51 are three small datasets. Different from previous datasets on classifying different action types (thus might be potentially inferred from single frames), Diving48 studies the three stages (takeoff, flight, and entry) of competitive diving. Thus achieving good results on Diving48 requires an understanding of the whole video clip. The license of each dataset allows academic use. SSV2 uses the 'Free Academic License'. HMDB51 is licensed under 'Creative Commons Attribution 4.0 International License'. 'The kinetics dataset is licensed by Google Inc. under a Creative Commons Attribution 4.0 International License.' We use the YouTube videos under the Fair Use.

Table 5. **Key statistics of video datasets** used in this paper. HowTo100M is used for pre-training while others are downstream datasets. The number of training/validation examples in HMDB51 and UCF101 are reported for the train-val split 1.

	HowTo100M	SSV2	Diving48	UCF101	HMDB51	Kinetics-400
Training	1238791	168913	15027	9537	3570	205418
Validation	-	24777	1970	3783	1530	17686
Number of Classes	-	174	48	101	51	400
Average Video Duration	6.5min	4s	6s	7s	4s	10s

E. Computational Cost

The pre-training takes around 8.9K V100 GPU hours. This computational cost is at the same level as ViT [19] supervised training (5.5K hours on ImageNet-21K [55] and 12.8K on JFT [60]). It is also at the same level of supervised training a model on Kinetics-400 dataset (6.4K for SlowFast [22], about 5.6K for TimeSformer-L [7]). For fine-tuning, SSV2, Diving48, UCF101, HMDB51, and Kinetics-400 take 1K, 200, 150, 40, 2K GPU hours, respectively. For analysis, the pre-training takes about 160 GPU hours. Besides the final model training, energy is also spent on tuning the model and finding the best configuration. As shown in Sec. F.2.3, our method is more robust to the hyperparameters.

F. Analysis

We also analyze the model's scalability and the effectiveness of our pre-training methods. To save computation, for all analyses, we use a smaller model (6-layer transformer with hidden dimension 512) and smaller input resolution (5 input frames with spatial size 128, i.e., T=5, S=128) throughout this section, unless otherwise stated. We also perform pre-training with fewer epochs (i.e., 10). For downstream tasks, we use the same input resolution as pre-training (i.e., T=5, S=128), and we use 2 temporal crops for inference. All results are reported on the train-val split 1 if applicable.

F.1. Scalability

In Table 6, we illustrate the scalability of our method with different model sizes (i.e., number of layers and hidden dimensions). Larger models have more parameters ('Params') and higher computational cost (measured by the normalized pre-training 'Speed'). To evaluate the pre-training tasks performance, we provide both pre-training metrics (mask-then-predict accuracy denoted by 'Mask-Accu.', and contrastive learning loss denoted by 'CL-Loss') and UCF101 downstream fine-tuning results. As the size of the model grows, the fine-tuning results show consistent improvement with the pre-training metrics. Note that for the last row in Table 6, we halve the attention head and MLP intermediate dimensions. We also illustrate the scalability over input resolution in Appendix G.2.

Table 6. Impact of **model size**. 'Speed' is the normalized pre-training speed measured by #videos/second on one V100 GPU. 'Mask-Accu.' and 'CL-Loss' are mask-then-predict accuracy and contrastive learning loss to indicate the pre-training performance. 'UCF101' is the fine-tuning accuracy on UCF101 dataset. By default, we use the configuration in the first line in our analysis. The configuration that produced the final results are underlined.

Layers	Dim	Params	Speed	Mask-Accu.↑	CL-Loss ↓	UCF101↑
6	512	29.4M	32.0	17.2	1.06	69.4
6	768	63.0M	21.0	17.7	1.03	75.0
12	512	54.7M	18.1	17.9	1.02	76.6
12	768	119.7M	11.2	18.4	1.00	78.1
<u>24</u>	<u>1024</u>	210.1M	5.0	18.7	0.98	78.5

F.2. Pre-Training Methods

F.2.1 The Impact of Pre-Training

Table 7. Impact of **pre-training tasks**. 'MP'=Mask-then-Predict, 'CL'=Contrastive Learning task.

MP	CL	Temporally-Heavy		Spatially-Heavy		
		SSV2	Diving48	UCF101	HMDB51	K400
✗	✗	1.2	10.0	41.3	19.0	41.0
✗	✓	32.5	26.3	57.1	30.7	47.0
✓	✗	41.4	37.2	68.3	35.3	53.7
✓	✓	41.1	37.5	69.4	37.8	54.5

We first compare different pre-training tasks and the non-pre-training results. As shown in Table 7, mask-then-predict is good at temporally-heavy datasets (SSV2, Diving48) while contrastive learning improves the spatially-heavy datasets.[4] We also compare with the non-pre-training results (the first row of Table 7) and observe that both tasks

[4]Empirically, we observe that the improvement of contrastive learning (CL) becomes higher when training with more epochs and larger architectures (as also shown in [12, 49]). With the Base model (but also using decreased training epochs), CL gives a 3% improvement on UCF101 over the pure mask-then-predict pre-training. In this section, we provide the comprehensive ablation studies based on the small model because of the limited budget.

Table 8. Impact of **masking strategy**. Models are pre-trained with only mask-then-predict.

Strategy	Frame Size S	Mask-Accu.↑	UCF101 ↑
block	128	17.6	68.3
i.i.d.	128	24.3	63.5 (-4.8)
block	256	11.2	69.5
i.i.d.	256	19.5	61.4 (-8.1)

Table 9. Impact of **masking ratio**. Models are pre-trained with only mask-then-predict. Default setup is underlined.

Strategy	#Blocks	Ratio	Mask-Accu.↑	UCF101 ↑
block	4	11.9%	17.9	66.8
<u>block</u>	<u>5</u>	<u>14.5%</u>	17.6	68.3
block	6	17.0%	17.3	67.3

significantly improve the results. We notice that these non-pre-training results are lower than previous from-scratch models, which might be caused by the difficulty in training video transformers [2,7] and the information loss in our input quantization process [52].

F.2.2 Mask-then-Predict

In this analysis, we exclude the contrastive learning loss (i.e., loss weight α=0) to avoid side effects.

Block Masking versus I.I.D. Masking. We first compare our proposed block masking strategy and the uniform i.i.d. masking strategy (discussed in Sec. 3.1 and illustrated in Fig. 2). As shown in Table 8, although the i.i.d. masking achieves higher pre-training mask-token-prediction accuracy ('Mask-Accu.'), it shows lower downstream results ('UCF101') than block masking. The higher mask accuracy is possibly due to the easier i.i.d. mask-then-predict task. We show in Appendix that simply copy-paste already yield reasonable reconstruction results. The existence of such a trivial solution potentially prevents the model from learning useful video representations for downstream tasks. Meanwhile, we also find that the model with larger input frame size 256 benefits more from the block masking strategy, because the adjacent tokens are closer in the original 2D image for these larger frames. Hence, the spatial locality is amplified.

Masking Ratio. In Table 9, we study the impact of masking ratio, by varying the number of masked blocks for block masking. Empirically, the result differences among different masking ratios are marginal and the original BERT's 15% masking ratio (with roughly 5 masking blocks) works slightly better. Thus we always select the number of mask blocks whose induced masking ratio is closest to 15%. The detailed choices of number of masking blocks are listed in Appendix.

Table 10. Impact of **maximum sampling distance** $d_{\max}$ (sec.) between two positive clips.

$d_{\max}$	Mask-Accu.↑	CL-Loss↓	UCF101↑
<u>∞</u>	17.2	1.06	69.4
30	17.3	0.77	69.0 (-0.4)
10	17.4	0.61	68.3 (-1.1)
0	17.5	0.41	66.7 (-2.7)

Table 11. Impact of **#negative samples**.

#samples	Mask-Accu.↑	CL-Loss↓	UCF101↑
<u>128</u> -1	17.2	1.06	69.4
256 - 1	17.1	1.30	69.2
512 - 1	17.2	1.56	70.4
1024 - 1	17.0	1.86	69.8

F.2.3 Contrastive Learning

Positive Sampling Distance. As illustrated in Sec. 3.2 and Fig. 2.(b), we uniformly sample positive clip pairs across the whole video without any distance restriction. To analyze the effect of such a sampling strategy, We perform a set of experiments by varying the maximum sampling distance d_{max} (in seconds) between two positive clips. The results are shown in Table 10. d_{max}=∞ denotes our default setup without any distance restriction. d_{max}=0 samples two same clips, and d_{max}=10 samples two positive clips with a maximum distance of 10 seconds. Although previous contrastive learning methods [23, 49] favor the sampling of temporal positives within a shorter range (e.g., maximum 36 seconds for uncurated videos in [23]), we observe a performance gain when using larger distance. We also want to emphasize that the results with d_{max}=10 and d_{max}=0 are not better than the model pre-trained with only mask-then-predict (UCF101 accuracy 68.3), which suggests that short-range contrastive learning does not improve upon our mask-then-predict task. This is potentially because our mask-then-predict already gives the model the ability to model local interactions, thus contrastive learning objective can only be useful when it focuses on longer-range interactions.

Number of Negative Samples. Previous constrastive learning methods [12, 14, 23] benefit from more negative samples. In this section, we show that the number of negative samples has less impact on our method when mask-then-predict task is added. As shown in Table 11, we use different contrastive learning sample sizes (i.e., n in Sec. 3.2) and always accumulate the gradients to 1024 samples before updating the parameters. Although increasing sample size makes the contrastive learning task harder (reflected by 'CL-Loss'), it does not show clear evidence of improving UCF101 downstream performance.

Input Masking as Augmentation. Most self-supervised visual representation learning methods [12, 13, 23, 29, 49]

Table 12. Impact of **mask augmentation in contrastive learning**. 'MP'=Mask-then-Predict. 'CL-Mask'=Use input mask in CL. Default setup is underlined.

MP	CL-Mask	Mask-Accu.↑	CL-Loss↓	UCF101↑
✗	✗	-	1.07	57.1
✗	✓	-	1.08	55.5
✓	✗	17.2	1.04	67.4
<u>✓</u>	<u>✓</u>	17.2	1.06	69.4

based on contrastive learning suffer from a large drop when removing strong spatial augmentations. In contrast, our pre-training does not use any spatial augmentations on raw frames. However, as we tie the input between mask-then-predict and contrastive learning to reduce computation cost, the random masking noise is naturally introduced. We here investigate its impact in Table 12. When pre-trained jointly with mask-then-predict, adding mask noise improves UCF101 accuracy by +2.0; however, when pre-trained without it, adding mask noise hurts the performance (-1.6). We hypothesize that this is due to the large input mismatches between pre-training and fine-tuning when mask-then-predict objective is not applied. Noisy masking creates 'holes' to the input token maps during pre-training, while for fine-tuning the input token maps are intact.

G. Additional Analysis Results

G.1. Model Architecture Comparisons

Attention Layouts. We here compare different alternative model architectures in Table 13. We consider the sparse attention as proposed in [15] and the sequential attention blocks as in [7]. The 'TxHxW' model is the basic attention module that takes the flattened tokens as input (of shape T ×H ×W). At each layer, each token attends to all other tokens. The 'T,HxW' model separates the temporal attention and spatial attention ('Divided Space-Time' in [7]). The 'T,H,W' model processes three attention sequentially ('Axial Attention' in [7]). The 'T, H—W' model is our default model that sequentially conduct temporal attention and spatial attention, where the spatial attention are parallel into the height attention and width attention. As shown in Table 13, 'T,H—W' reaches a balance between speed and accuracy.

Pre-Layer-Normalization vs. Post-Layer-Normalization. Besides the architectures listed above, we also consider the pre-layer-norm (used in GPT and ViT) and post-layer-norm (used in BERT) variation. We empirically find that post-layer-norm architecture is better for our pre-training tasks as shown in Table 13 (comparing the last 2 columns).

G.2. Input Resolution

In Table 14, we show model scalability over input resolution (i.e., #frames T and frame size S). With the same frame size S, longer clips perform better than shorter clips (e.g., T=10, S=128 is better than T=5, S=128). With the same number of input frames T, larger frame size improves the performance (e.g., T=10, S=256 is better than T=10, S=128). For each pre-training resolution, we also try to fine-tune under a full-resolution with T=10, S=256 (denoted as 'UCF101-Full-Reso.'). As in pre-training, fine-tuning with larger resolution generally improves the results. Although longer and smaller clips (T=10, S=128) show better results than shorter and larger clips (T=5, S=256) when using the same pre-training and fine-tuning resolutions, they show different trends with the full-resolution fine-tuning. Increasing frame size during fine-tuning (the second block in Table 14) only improves the UCF101 result by 0.4, while increasing the clip length (the third block) improves the UCF101 result by 3.8. These results call for a need of pre-training with large spatial size, and we follow this practice in our large-scale experiments as in Sec. 4.2.

G.3. Noisy Masking for Mask-then-Predict

Our default masking strategy replaces all masked tokens with a special `[MASK]` symbol. We also experiment with BERT's masking strategy that only replaces 80% of masked tokens to the MASK symbol. For other tokens, 10% are randomly sampled from the 'vocabulary' and 10% are kept the same. For smaller experiments, the two masking strategies show similar results. However, this BERT's noisy masking strategy has lower convergence stability on the larger model pre-training. The pre-training diverges after about 10 epochs (out of the 100 epochs).

G.4. Masking Ratio for Block-Masking and I.I.D. Masking

We test the effect of different masking ratios. In the main text, we control the number of blocks for block masking. In Table 15, we here also show the results of matched masking ratio for i.i.d. masking for completeness. Empirically, the result differences among various masking ratios are marginal and the original BERT's 15% masking ratio (with roughly 5 masking blocks) works slightly better. Thus we always select the number of mask blocks whose induced masking ratio is closest to 15%. For all masking ratios, block masking shows significantly better results than the i.i.d. masking.

G.5. Impact of Contrastive Learning Loss Weight

In Table 16, we show the impact of loss weight α (see Sec. 3.3). Since the loss have been calibrated by multiplying the temperature, α=1 shows stable results and α=0.5 is

Table 13. Results of **different attention-module layouts and layer-normalization positions**. 'Speed' is the normalized pre-training speed (i.e., number of samples / GPU / second). Models are pre-trained on HowTo100M for 10 epochs. The result numbers represent UCF101 accuracy.

	Params	Speed	Pre-LayerNorm	Post-LayerNorm
TxHxW	23.1M	12.6	-	65.9
T,HxW [7]	27.1M	20.0	-	69.0
T,H,W	35.8M	26.4	69.0	69.6
T,H—W (ours)	29.4M	32.0	67.6	69.4

Table 14. Impact of **input resolutions** T **and** S. 'Mask-Accu.' and 'CL-Loss' are the pre-training metrics. 'UCF101' indicates the UCF101 fine-tuning results with the pre-training resolution. 'UCF101-Full-Reso.' indicates the full-resolution fine-tuning with T=10 and S=256.

#frames T	Frame Size S	Params	Pre-train Speed	Mask-Accu.↑	CL-Loss↓	UCF101↑	UCF101-Full-Reso.↑
5	128	29.4M	32.0	17.2	1.06	69.4	73.8
10	128	29.4M	16.5	17.2	0.96	74.2	74.6
5	256	29.4M	8.4	10.8	0.93	72.9	75.7
10	256	29.4M	4.4	10.6	0.85	78.1	78.1

Table 15. Impact of **masking ratio**. All models are pre-trained with only mask-then-predict task. #Blocks is the number of masking blocks. Default setup is underlined.

Strategy	#Blocks	Ratio	Mask-Accu.↑	UCF101 ↑
Block	4	11.9%	17.9	66.8
<u>Block</u>	<u>5</u>	<u>14.5%</u>	17.6	68.3
Block	6	17.0%	17.3	67.3
i.i.d.	-	11.9%	25.6	64.5
i.i.d.	-	14.5%	24.3	63.5
i.i.d.	-	17.0%	24.0	64.0

Table 16. Impact of **contrastive learning loss weight** α. Default setup is underlined.

α	Mask-Accu.↑	CL-Loss↓	UCF101↑
0.0	17.6	-	68.3
0.5	17.5	1.07	70.2
<u>1.0</u>	17.2	1.06	69.4
2.0	16.9	1.05	68.0
∞*	-	1.07	57.1

slightly better. Setting α=2.0 will let the model to focus mostly on contrastive learning task and its result is worse than pure mask-then-predict pre-training (i.e., α=0.0). We also list the pure contrastive learning pre-training results here (denoted as α=∞* but it excludes the mask-then-predict loss and set α=1.0) for reference.

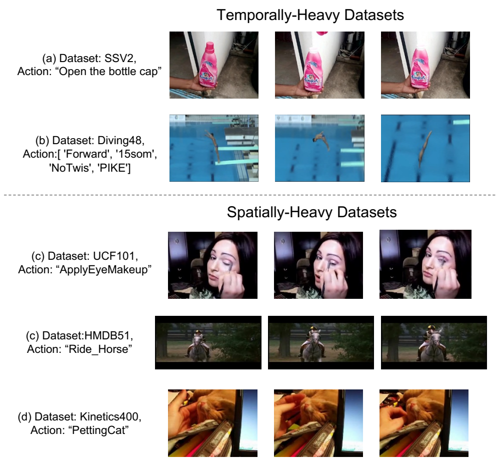
Temporally-Heavy Datasets
(a) Dataset: SSV2, Action: "Open the bottle cap"
(b) Dataset: Diving48, Action:['Forward', '15som', 'NoTwis', 'PIKE']
Spatially-Heavy Datasets
(c) Dataset: UCF101, Action: "ApplyEyeMakeup"
(c) Dataset:HMDB51, Action: "Ride_Horse"
(d) Dataset: Kinetics400, Action: "PettingCat"

Figure 3. Data samples from temporally-heavy and spatially-heavy datasets. While temporally-heavy datasets need the temporal information to make decisions, most actions in spatially-heavy datasets could be inferred from just a single frame.

H. Visualizations

H.1. Temporally-Heavy vs. Spatially-Heavy Datasets

We illustrate the differences between temporally-heavy and spatially-heavy datasets in Fig. 3. We here show equally-distributed frames from the video and the label of the video clip. Note that we do not cherry-pick the data but aim for showing the nature of each dataset. Overall, understanding in temporally-heavy datasets needs temporal modeling, whereas the action labels of spatially-heavy datasets

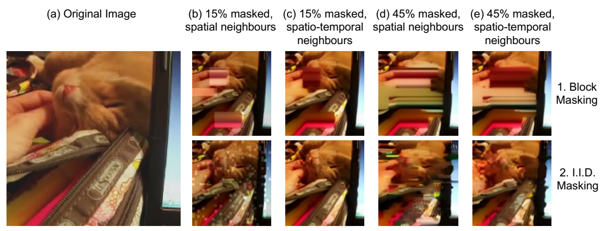

(a) Original Image
(b) 15% masked, spatial neighbours
(c) 15% masked, spatio-temporal neighbours
(d) 45% masked, spatial neighbours
(e) 45% masked, spatio-temporal neighbours
1. Block Masking
2. I.I.D. Masking

Figure 4. Nearest-neighbour reconstruction of *block masking* and *i.i.d masking*. We mask tokens at different ratios and reconstruct them by simply copying their spatial or spatio-temporal neighbours. Even under heavy masking (e.g., 45% masked), this simple reconstruction strategy still yields a reasonable results for *i.i.d masking*, e.g., we can easily recognize the action 'petting cat' from the reconstructed images, especially the one reconstructed from spatio-temporal neighbours. However, this becomes significantly more difficult when using *block masking*.

could be inferred from a single frame. To understand the SSV2 [28] example in Fig. 3.(a), the model needs to understand the causality, i.e., the order of the frames decides the action label. In Fig. 3.(b), the competitive diving dataset Diving48 [42] also requires considering nearly all frames to make the decision. However, for the spatially-heavy datasets (UCF101 [57], HMDB51 [39], Kinetics-400 [10]), the action label could be inferred from any single sampled frame. These observations result in the pretty high frame-level accuracy (i.e., not modeling temporal interactions) in Sec. 4.2.

H.2. Masking Strategy Comparisons

We propose to use block masking (in Sec. 3.1) since i.i.d. masking may lead to trivial solutions for the mask-then-predict task given the strong localities in videos. We illustrate this point in Fig. 4 with a simple copy-paste reconstruction method. Specifically, after masking, we first replace the masked tokens with their *nearest visible neighbours* (i.e., the unmasked token that has the shortest distance in spatial or spatio-temporal domain), and then forward the reconstructed tokens to the VQ-VAE decoder to generate the RGB images. For the default 15% masking ratio, i.i.d. masking is recoverable while block masking causes striped noisy patterns.[5] We also test with the extreme case of masking 45% tokens (in Fig. 4 (d), (e)). The block-masked images are hard to reconstruct, however, some objects in reconstructed images from i.i.d. masking are still recognizable. When comparing images under the same masking strategy, recovered images using spatio-temporal neighbours is better than using only spatial neighbours, especially when comparing the images under 45% i.i.d. masking (i.e., (d).2 and (e).2 in Fig. 4). Overall, these results indicate that using i.i.d. masking in mask-then-predict task has a potential trivial solution by copying the neighbourhood, while block-masking resolves this issue.

[5]We highlight the masking region in Fig. 4(b) and show the raw RGB images in other cases.

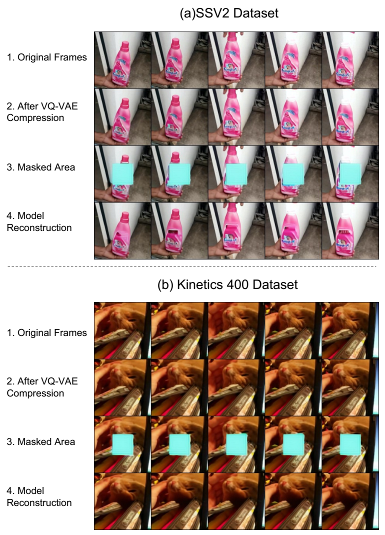

Figure 5. Masked-token model reconstruction for SSV2 and Kinetics-400 datasets. Comparing 1. and 4., our model could redraw temporally-consistent and spatially-plausible patches for the masked regions.

H.3. Model Reconstruction

Since our model is trained with mask-then-predict task, it is able to reconstruct masked tokens. In this section, we showcase the reconstructed video frames by our final model (i.e., 24 layers, 1024 dimensions, 5 clip length, and 256 frame size). As shown in Fig. 5, we provide two examples from the SSV2 and Kinetics-400 dataset. We uniformly sample 5 consecutive frames from the video at 1 frame per second. We show the original frames in the first rows (Fig. 5.(a).1, (b).1). As illustrated in Sec. H.1, the temporally-heavy SSV2 dataset has object motions between frames while the spatially-heavy Kinetics-400 dataset has almost static frames. In the second rows, we show the images after VQ-VAE compression. To do this, we first use VQ-VAE encoder to encode the images, and then use VQ-VAE decoder to reconstruct the images, without any corruptions in between. We see that there is some information loss caused by the VQ-VAE compression (e.g., the text 'comfort' in Fig. 5.(a).1). It potentially contributes to relative lower results on spatially-heavy datasets. In the third and fourth rows, we illustrate the masked area and the prediction from our model. As shown in Fig. 5.(a).4, our model could faithfully redraw the shape and texture of the object. As shown in Fig. 5.(b).4, the shape of the cat's head is pretty similar to the original frames while the shading is different (but still consistent in different frames).

I. Reproducibility statement.

The code to reproduce the results in this paper is submitted in the supplementary material and will be made public. The code is runnable and contains the scripts with faithful hyperparameters for our experiments. We include comprehensive instructions about the feature extraction, pre-training, and fine-tuning. A detailed "readme" file is attached in the codebase, and we will publicly release the pre-trained weights as well.

J. Ethical considerations and limitations.

The main purpose of this work is to design a video pre-training method to capture internal interactions. In real life, a lot of tasks are temporally-heavy such that the task completion relies on understanding the past. Video understanding is a proxy to these embodied studies eventually and thus could one day benefit our daily life. Our work is also potentially useful for recovering corrupted videos (but this could also be possibly misused, hence we recommend careful and safe use of this technology, including previous works). In this paper, we mainly consider the action classification tasks with different characteristics (i.e., spatially-heavy and temporally-heavy) and we show the recovering ability of our model. It's also possible to employ VIMPAC backbone to video detection tasks where tokens' outputs can be viewed as anchors.

The DALL-E VQ-VAE code and model are published under MIT license. We are among the first line of work that use masked token reconstruction, etc. as a self-supervised learning approach for vision, and we do agree the the use of VQ-VAE tokens might limit the models' ability in certain aspects, such as spatial info loss. Future work could explore combining the techniques from BEiT [4] for a more capable approach. Meanwhile, token-level approach has its unique advantage of generative modeling (as shown in VQ-GAN [21], DALL-E [52]), more robust to the input noise, and has the possibility to transfer to other modality (e.g., text; since they share the same types of input). This cross-modality transferability is another future direction that we consider.